http://eprints.gla.ac.uk/233136/

Automatic Shock Detection, Extraction and Fitting in High Speed Schlieren and Shadowgraph Visualization

SCHOLARONE™
Manuscripts

Automatic Shock Detection, Extraction and Fitting in Schlieren and Shadowgraph Visualization

Guoshuai Li[1]

China Aerodynamics Research and Development Center, Mianyang, 621000, China

Konstantinos Kontis[2]

University of Glasgow, School of Engineering, Glasgow, G12 8QQ, UK

Zhaolin Fan[3]

China Aerodynamics Research and Development Center, Mianyang, 621000, China

Nomenclature

D = distance between the shock tube end and the plate surface

f = image value in its spatial domain

F = image value in its frequency domain

G_x = image gradient in x direction

G_y = image gradient in y direction

K = filter kernel

M = Mach number

M_s = shock Mach number

T = threshold value

T_H = high threshold value

T_L = low threshold value

WA = weighted average value

I. Introduction

SCHLIEREN and shadowgraph techniques have been increasingly used to visualize unsteady shock-related

phenomena such as moving shock waves, shock reflections, dynamic shock-shock interactions, and shock-boundary

layer interactions [1-5]. In these cases, large data sets are generally produced. Therefore, the ability to automatically

---
[1] Assistant Professor, High Speed Institute; gli2221132@126.com (Corresponding Author).
[2] Professor, Department of Aerospace Science; kostas.kontis@glasgow.ac.uk, Fellow AIAA.
[3] Professor, fanzhaolin@cardc.cn.

detect, extract, and track shock waves from a large number of experimental or numerical shadowgraph and schlieren sequences has increased rapidly in the last decades [6-9].

Estruch et al. [10] proposed a method to evaluate shock wave unsteadiness by point tracking based on edge images. Although the shock motion can be estimated, other flow properties such as shock distortion and inclination angle are not attainable. Also, software for extracting flow features from schlieren sequences was developed at the High Enthalpy Shock Tunnel in Göttingen [11]. Hough transform and its variants were used to track the model motion and calculate the oblique shock angle. However, image processing algorithms employed by the software are not fully rule-based and the extraction process requires significant user involvement. Additionally, T. Fujimoto et al. [6] combined the Canny edge detection algorithm and Rankine-Hugoniot relations to detect shock waves automatically without threshold values that were required for the traditional Canny algorithm. Furthermore, N. T. Smith et al. [12] developed a tentative approach based on computer vision techniques, which provides an empirical estimate of oblique structure angles by scanning image lines for two edge points. They also [7] proposed a method to detect the motion of large-scale shock wave structure by tracking the sharp model tip and the intersection point of shock waves based on fused feature identification algorithms. The curvature scale space (CSS) representation was adopted to isolate shock contours in their study and a measurement success rate over 95% was obtained across several thousand frames.

This paper presents an image processing scheme based on advanced computer vision algorithms, to provide the capability of fully automatic shock detection and further improve the accuracy.

II. Proposed Image Processing Scheme

A. Image pre-processing

First, all the schlieren or shadowgraph sequences are converted into 8 bit grayscale images for improving the calculating efficiency, no matter what original format and depth they are.

Background image subtraction in the frequency domain is performed then to achieve pure images representing the flow field. The primary process involves converting the background image captured without the flow and test images with the flow from the spatial domain into the frequency domain by the Fourier Transform [13], subtracting the background image from test images in the frequency domain, and finally converting the subtracted test images back into the spatial domain by inverse Fourier transform (IDFT) [13]. However, the test model body and the out-of-measurement region are also removed during the above process. A simple but effective image segmentation

2

Submitted to AIAA Journal. Confidential - Do not distribute.

algorithm based on global thresholding can be implemented to isolate the test model body and the out-of-measurement region from the background image. This scheme provides two algorithms, Otsu thresholding [14] and Triangle thresholding [15], to calculate the global threshold value automatically.

In time-resolved shadowgraph and schlieren measurement, the spatial resolution of result images is usually small to achieve a higher frame rate, which will affect the accuracy of shock detection and extraction. Lanczos upsampling algorithm [16] involving a trade-off between efficiency, smoothness and sharpness is adopted to interpolate the test images.

Finally, image filter is conducted. The core of image filtering is the operation of convolution [13]:

$$g(x, y) = K * f(x, y) = \sum_{s=-a}^{a} \sum_{t=-b}^{b} K(s,t) f(x-s, y-t) \tag{1}$$

where $g(x, y)$ is the filtered image, $f(x, y)$ is the original image, K is the filter kernel, a and b refer to the size of the kernel matrix. The convolution operation that scans the whole image is quite time-consuming, especially when dealing with a large set of images. In this study, performing a 3×3 median filter and 5×5 bilateral filter subsequently is recommended for most of the cases. A median filter with a small kernel can effectively remove the salt-and-pepper noise [17] in which corrupted pixels take the maximum and minimum value. The bilateral filter is capable of removing Gaussian noises while preserving edges [18]. Although a larger kernel size yields a better denoising effect for the bilateral filter, small kernel sizes of less than 7 are generally adopted in real-time applications due to a compromise between the calculating efficiency and the denoising effect.

B. Contour detection

Contour represents a curve joining all the continuous points along the boundary that have the same intensity value and is an effective tool for object detection and shape analysis in the computer vision community [19-21]. In this study, contours related to shock waves are detected from binary images calculated by a modified Canny algorithm or an adaptive threshold algorithm.

Canny edge detection algorithm has been widely used in shock wave detection and extraction in previous studies [6, 7, 10, 12, 22] due to its incorporation of a low error rate, a single response criterion, and inclusion of scale. However, in the conventional Canny algorithm, a high threshold value T_H and a low threshold value T_H were typically required to be adjusted empirically for each specific application [6]. The current scheme utilizes Otsu algorithm [14] to evaluate the above two threshold values automatically. Specifically, the threshold value

automatically calculated by Otsu algorithm is set to T_H and the low threshold value T_L is 1/2 of the high threshold value T_H.

Adaptive threshold, in which the threshold value at each pixel is different and determined by the neighboring pixels around the target pixel, is the other algorithm used for producing binary images for contour detection. To calculate the threshold value $T(x, y)$ at a pixel (x, y), a $d\times d$ region around the pixel is selected first. The next step is to calculate the average (mean) or the Gaussian weighted average of all the pixels that lie in the $d\times d$ box. This weighted average value is set to the threshold $T(x, y)$ of the pixel (x,y).

Each contour detected from the binary images calculated by the modified Canny or adaptive threshold algorithm is stored as a vector of pixel coordinates. A tree algorithm [23] retrieving all contours and reconstructing a hierarchy of all nested contours is used for contour retrieval.

C. Shock extraction

First, the properties of each contour, like hierarchy, size, area, perimeter, centroid, and bounding box are calculated. One or several of these properties that can distinguish between contours related to shock waves and pseudo contours not corresponding to true flow structure are selected as the rule for shock extraction. Then the shock extraction is accomplished by removing all the pseudo contours according to their property values. The success rate depends on how many images follow the rule for shock contour extraction.

D. Shock contour fitting and post-analysis

On some occasions, especially for low signal-noise ratio images, some points that do not belong to shock waves are kept. To improve the accuracy of shock detection and extraction, the extracted shock contour can be fitted using polynomial functions in the present scheme. Points not corresponding to shock waves are removed and then investigations involving the shock propagation speed, shock distortion, and shock angle can be conducted based on time-resolved schlieren and shadowgraph sequences.

III. Verification of the Proposed Image Processing Scheme

A. Facility and Experimental setup

To validate the proposed scheme, it is applied to process the low signal-to-noise ratio (SNR) and small spatial resolution (312×260-pixel) shadowgraph images from several supersonic starting jet tests [5, 24]. The schematic diagram of the experimental setup is shown in Fig. 1. A circular (inner diameter ID = 22 mm, driven section length

4

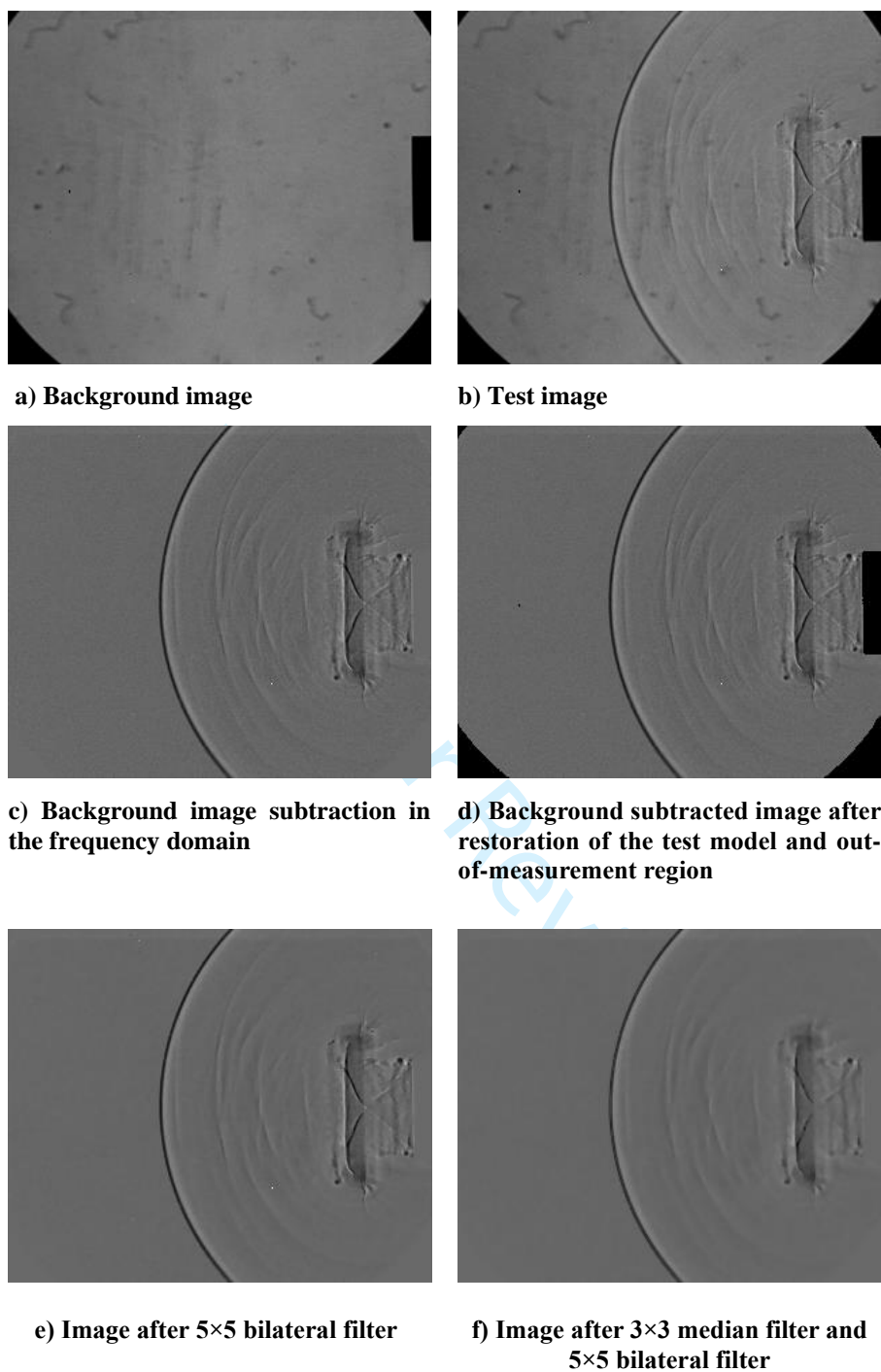Submitted to AIAA Journal. Confidential - Do not distribute.

L = 330 mm) and a square (side length *d* = 22 mm, *L* = 330 mm) open-ended shock tube driven by detonation

transmission tubing [5] were employed to simulate the circular and square supersonic starting jets respectively. An

HPV-1 Shimadzu high-speed camera having a recording speed up to 1Mfps was used, which can record up to 102

images each run at a fixed spatial resolution of 312 ×260. The validation shadowgraph experiment involves: (i) flow

visualization of circular supersonic starting jets and their impingement over flexible surfaces, (ii) flow visualization

of square supersonic starting jets and their impingement over flexible surfaces, (iii) shock velocity measurement.

Over 2000 images from 60 runs were processed automatically by the proposed scheme. A dynamic pressure

transducer (Kulite Semiconductor Products, Inc., model: XTE-190M, natural frequency: 175 kHz) was placed at 50

mm from the shock tube open end to measure the pressure history in the driven section. The shock Mach number M_s

calculated by the overpressure magnitude based on normal shock wave theories [5] is compared to that evaluated by

shadowgraph sequences processed by the present image processing scheme.
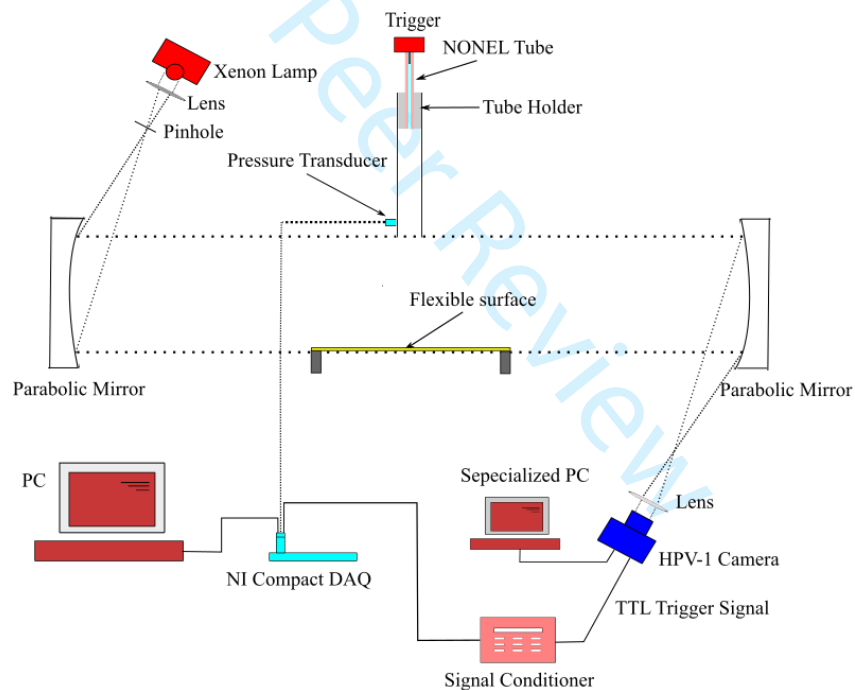
Fig. 1 Schematic of the experimental setup

It is worth noting that different frame rates (250 kfps and 500kfps respectively) were adopted at each test to

validate the capability of the proposed scheme for processing images in different noise levels (lower signal-to-noise

ratio at a higher frame rate). Additionally, the measurement size of the first two shadowgraph tests is 105.7mm ×

88mm. To improve the accuracy of shock velocity evaluation, the visualization size was reduced to 20.9mm ×

17.4mm in the third test, having a resolution of 0.067mm/pixel.

5

Submitted to AIAA Journal. Confidential - Do not distribute.

B. Results and analysis

a) Background image

b) Test image

c) Background image subtraction in the frequency domain

d) Background subtracted image after restoration of the test model and out-of-measurement region

e) Image after 5×5 bilateral filter

f) Image after 3×3 median filter and 5×5 bilateral filter

Fig. 2 Preliminary processing of a shadowgraph image from a free circular supersonic starting jet at a frame rate of 250 kfps (M_s=1.57)

Generally, some preliminary processing steps should be performed before the implementation of shock detection to improve the detection accuracy. Figure 2 illustrates the preliminarily processing results of a shadowgraph image from a circular supersonic starting jet [5]. Figures 2(a) and (b) present the wind-off background image and wind-on
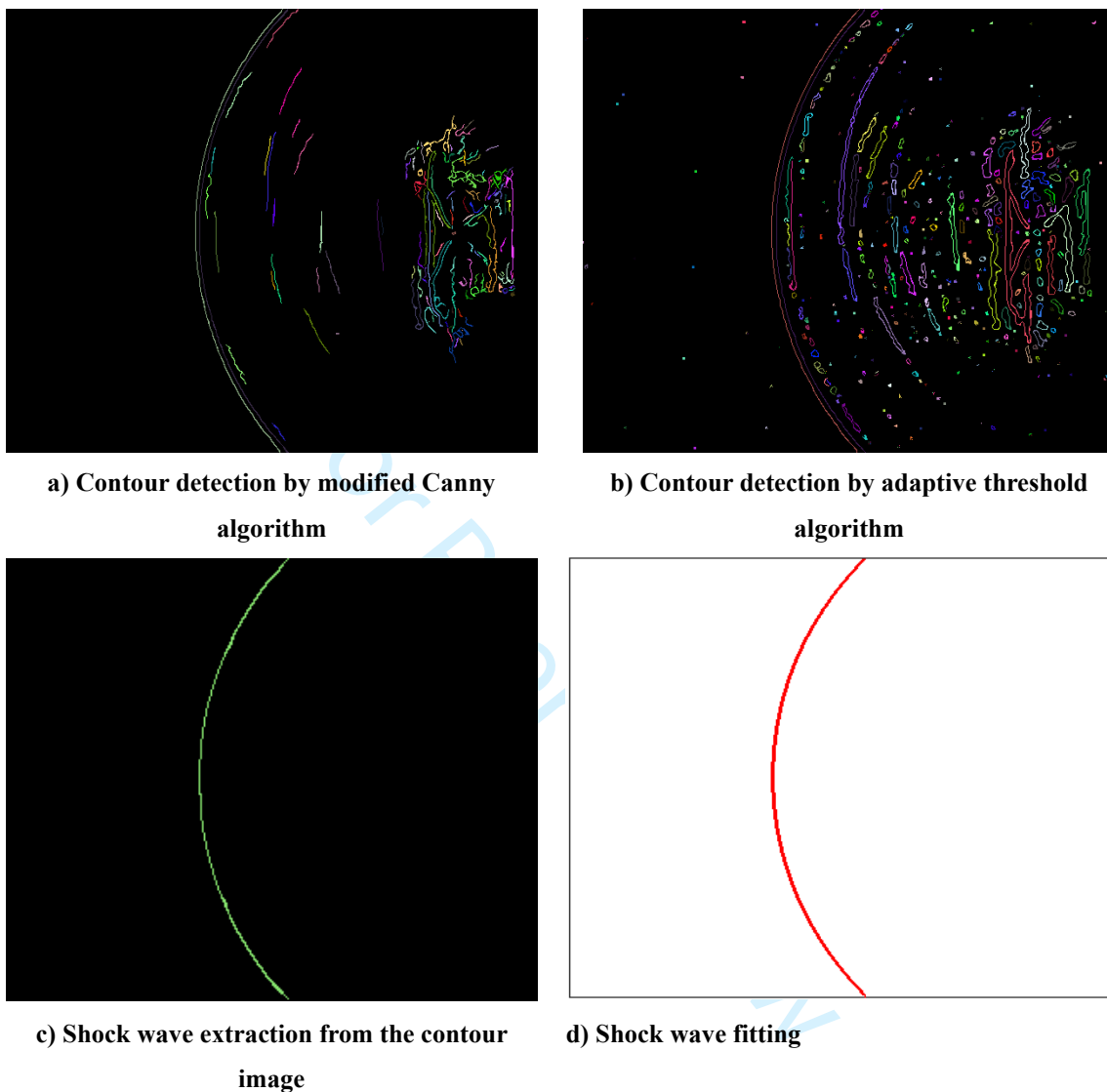
test image respectively. First, all the shadowgraph images were converted from 12 bit grayscale images into 8 bit grayscale images for improving calculating efficiency. Then, the background image was subtracted from test images in the frequency domain. As shown in Fig. 2(c), the area representing the shock tube and out-of-measurement region is eliminated by the background image subtraction. Also, contamination existed both in the background image and test image because of uncleaned lens and mirrors is removed, making the flow features more prominent. It is worth noting that the subtraction algorithm is robust to the overall intensity variation of shadowgraph images and the light uniformity of the xenon lamp used in this study is assumed steady for all the 102 recorded images at each run. Therefore, only one background image was acquired for each run.

The area representing the shock tube and out-of-measurement region can be isolated and restored via performing image segmentation on the background image. Fig. 2(d) presents the test image after background subtraction and restoration of the shock tube and out-of-measurement region through a global thresholding segmentation algorithm. The global threshold value is 93, which was automatically calculated from Fig. 2(a) by Ostu algorithm [14, 23]. Figure 2(e) displays the image filter result of Fig. 2(c) through a 5×5 bilateral filter. Compared Fig. 2(c) with Fig. 2(e), it can be seen that the bilateral filter is capable of removing the Gaussian noise effectively while preserving edges. However, the bilateral filter is not good at filtering the salt and pepper noise. Figure 2 (f) illustrates the filter result combining a 3×3 median filter and a 5×5 bilateral filter. It appears that the salt-and-pepper noise is eliminated effectively, however, edges become more blurred to some extent because of the nonlinear median filter.

Figures 3(a) and (b) depict the contour detection results of image Fig. 2(f) processed by the modified Canny algorithm and the adaptive threshold algorithm respectively. These two methods are both capable of detecting main flow features from the shadowgraph image including the primary shock wave, secondary shock waves, vortex ring, and oblique shock wave structure [4, 5]. However, more details such as weak secondary shock waves can be detected by the adaptive threshold algorithm with more small pseudo contours (Fig. 3(b)).

To investigate the distortion and propagation of the primary shock wave, contours not corresponding to the primary shock should be removed. For the current shadowgraph sequence visualizing the free circular supersonic starting jet, only the contour size is adopted as the rule for shock contour extraction and the largest contour is extracted as the primary shock wave. Figure 3 (c) shows the contour extraction result calculated from Fig. 3(a). In Fig. 3 (a), there are 133 contours in total (different contours are shown in different colors). The contour of the outer primary shock wave is the largest one with a size of 552 points. Since shock contours are the largest ones in all

shadowgraph sequences in this study, the measurement success rates of validation cases described in Section III.A are 100%. However, it may differ in other applications.

a) Contour detection by modified Canny algorithm

b) Contour detection by adaptive threshold algorithm

c) Shock wave extraction from the contour image
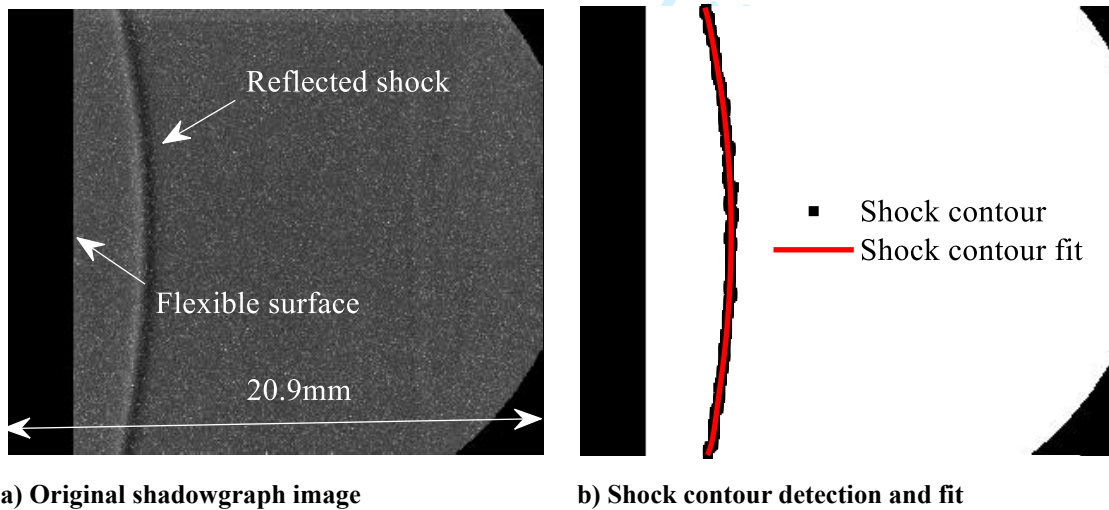

d) Shock wave fitting

Fig. 3 Shock detection, extraction and fitting

At the level of pixel inspection, although the image coordinates of each pixel on the outer shock wave are extracted, the discrete curvature is still a little noisy at a small scale (Fig. 3(c)) rather than a smooth one because some points that do not belong to the shock wave are kept. To solve this problem, the extracted shock contour was fitted using a fourth-order polynomial function in a sub-pixel accuracy. As shown in Fig. 3(d), redundant points are removed effectively. Afterwards, investigations involving the shock unsteadiness, shock distortion, and shock angle can be conducted based on the fitted shock contours from time-resolved shadowgraph sequences.

8

Submitted to AIAA Journal. Confidential - Do not distribute.
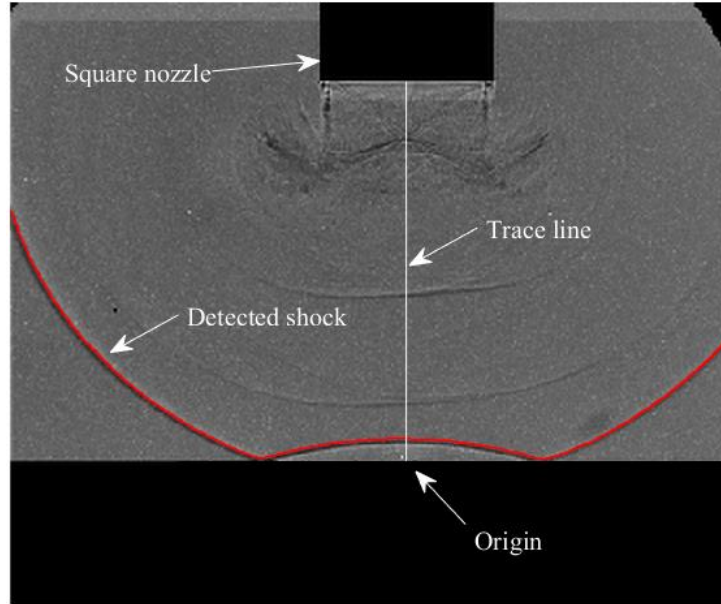
Fig. 4 Shock detection result of a shadowgraph image during the process of square supersonic starting jet impingement at a frame rate of 500 kfps (M_s=1.53, the distance from the shock tube end to flexible surface D=55mm)

Fig. 4 shows the shock wave detection result of a shadowgraph image during the process of a square supersonic

starting jet impingement at a frame rate of 500 kfps. Because of a higher frame rate, the signal to noise ratio of Fig.4

is lower than that of Fig.2 (d). As shown in Fig. 4, following the image processing procedure described in section II,

the reflected shock wave is detected and extracted effectively.

a) Original shadowgraph image   b) Shock contour detection and fit

Fig. 5 Shock detection and fitting results of a shadowgraph image for calculating the velocity of the reflected shock wave at a frame rate of 500 kfps (M_s=1.27, D=30mm)

Figure 5 presents the shock detection and fitting results of a shadowgraph image during the process of a square

supersonic starting jet impingement in the third shadowgraph test. As illustrated in Fig. 5, the shock wave in the

9

Submitted to AIAA Journal. Confidential - Do not distribute.

present shadowgraph image is significantly thicker than those in Fig. 2 and Fig 4 due to a much smaller visualization size. In this study, the shock detection uncertainty is evaluated by the pixel displacements between the detected and fitted shock contours. In the first two cases, the shock detection error is generally less than 1.5 pixels. However, as shown in Fig. 5(b), the error can be 3-5 pixels at some locations due to the low signal-to-noise ratio and low image contrast. In such cases, contour fitting becomes more crucial for improving the accuracy of shock detection and extraction.

The instantaneous locations of the primary shock wave during the process of supersonic starting jet impingements can be achieved by processing shadowgraph sequences at each run in the third shadowgraph test. Figure 6 illustrates the evolution of the primary shock wave tip detected from shadowgraph sequences during the process of a square supersonic starting jet impingement at a frame rate of 250 kfps. The elapsed time after the primary shock wave from the shock tube exit reaches the flexible surface is defined as t. The first derivative of the curve in Fig. 6 refers to the shock propagation velocity. It can be obtained from Fig. 6 that the velocity of primary shock from the square starting jet is 529.17m/s and the velocity of reflected shock wave declines to 364.54m/s.
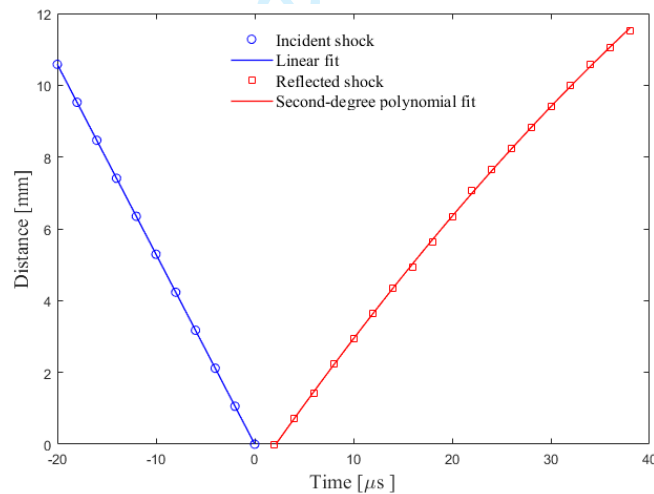
Fig. 6 Time evolution of the shock wave tip during the process of a square supersonic starting jet impingement at a frame rate of 250 kfps (M_s=1.53 and D=30mm)

Table 1 gives the comparison of shock wave Mach numbers from the free supersonic starting jets calculated by the shadowgraph sequences and peak overpressure magnitudes. Shadowgraph images were automatically processed by the proposed scheme (Section II) and normal shock theories [5] are used to estimate the shock Mach numbers from overpressure magnitudes in the driven section. It can be seen from Table 1 that the dispersion of shock velocities calculated by these two methods is less than 2%.

Table 1 Comparison of shock wave Mach numbers M_s calculated by shadowgraph sequences and peak overpressure magnitudes

M_s by peak overpressure	M_s by shadowgraph	ΔM	Dispersion
1.29	1.27	-0.02	1.6%
1.39	1.38	-0.01	0.7%
1.48	1.46	-0.02	1.4%
1.58	1.57	-0.01	0.6%

IV. Conclusion

To automatically and accurately detect, localize and track fluid features from large measured or computed shadowgraph and schlieren data sets, this paper presents an image processing scheme involving background subtraction in the frequency domain, image segmentation, filtering, resampling, edge detection, adaptive threshold, contour detection, shock extraction, and fitting. The conventional Canny edge detection algorithm is modified to calculate the double threshold values automatically. Additionally, the adaptive threshold algorithm provides the other option for contour detection. To improve the shock detection accuracy, extracted shock contours are fitted using polynomial functions. Over 2000 noisy shadowgraph images at a small spatial resolution involving free supersonic starting jets and their impingement over flexible surfaces were automatically processed by the proposed image processing scheme to investigate shock propagation, reflection, and distortion. Results show that the scheme proposed in this paper is applicable and effective for shadowgraph sequences in different noise levels. Furthermore, the comparison of shock velocity evaluated by the overpressure magnitude based on normal shock theories and velocity calculated by shadowgraph sequences are in good agreement. Next, more advanced image processing algorithms will be tested and applied to enhance the capability and robustness of this scheme.

Acknowledgments

References

[1]   G. S. Settles and M. J. Hargather, "A Review of Recent Developments in Schlieren and Shadowgraph Techniques," *Measurement Science and Technology,* vol. 28, no. 4, 2017.

https://doi.org/10.1088/1361-6501/aa5748

[2]   D. Daub, S. Willems, and A. Gülhan, "Experiments on the Interaction of a Fast-Moving Shock with an Elastic Panel," *AIAA Journal,* vol. 54, no. 2, 2016, pp. 670-678.

https://doi.org/10.2514/1.J054233

[3]   H. Zare-Behtash, K. Kontis, N. Gongora-Orozco, and K. Takayama, "Shock Wave-Induced Vortex Loops Emanating from Nozzles with Singular Corners," *Experiments in Fluids,* vol. 49, no. 5, 2010, pp. 1005-1019.

https://doi.org/10.1007/s00348-010-0839-7

[4]   E. F. Médici and G. P. Waite, "Experimental Laboratory Study on the Formation of Multiple Shock Waves Observed During Volcanic Eruptions," *Geophysical Research Letters,* vol. 43, no. 1, 2016, pp. 85-92.

https://doi.org/10.1002/2015GL066426

[5]   G. Li, T. Ukai, and K. Kontis, "Characterization of a Novel Open-Ended Shock Tube Facility Based on Detonation Transmission Tubing," *Aerospace Science and Technology,* 2019.

https://doi.org/10.1016/j.ast.2019.105388

[6]   T. Fujimoto, T. Kawasaki, and K. Kitamura, "Simpler Method of Shock Wave Detection by Using Canny Method," 2018 Fluid Dynamics Conference, 2018.

https://doi.org/10.2514/6.2018-4274

[7]   N. T. Smith, M. J. Lewis, and R. Chellappa, "Detection, Localization, and Tracking of Shock Contour Salient Points in Schlieren Sequences," *AIAA Journal,* vol. 52, no. 6, 2014, pp. 1249-1264.

https://doi.org/10.2514/1.J052367

[8]   H. Akhlaghi, A. Daliri, and M. R. Soltani, "Shock-Wave-Detection Technique for High-Speed Rarefied-Gas Flows," *AIAA Journal,* vol. 55, no. 11, 2017, pp. 3747-3756.

https://doi.org/10.2514/1.J055819

[9]   Z. Wu, Y. Xu, W. Wang, and R. Hu, "Review of Shock Wave Detection Method in CFD Post-Processing," *Chinese Journal of Aeronautics,* vol. 26, no. 3, 2013, pp. 501-513.

https://doi.org/10.1016/j.cja.2013.05.001

[10]   D. Estruch, N. J. Lawson, D. G. MacManus, K. P. Garry, and J. L. Stollery, "Measurement of Shock Wave Unsteadiness Using a High-Speed Schlieren System and Digital Image Processing," *Review of Scientific Instruments,* vol. 79, no. 12, 2008, p. 126108.

https://doi.org/10.1063/1.3053361

[11]   J. Wolfram and J. Martinez Schramm, "Pattern Recognition in High Speed Schlieren Visualization at the High Enthalpy Shock Tunnel Göttingen (HEG)," New Results in Numerical and Experimental Fluid Mechanics VII, 2010. https://doi.org/10.1007/978-3-642-14243-7_49

[12]   N. T. Smith, M. J. Lewis, and R. Chellappa, "Extraction of Oblique Structures in Noisy Schlieren Sequences Using Computer Vision Techniques," *AIAA Journal,* vol. 50, no. 5, 2012, pp. 1145-1155. https://doi.org/10.2514/1.J051335

[13]   R. Szeliski, *Computer Vision : Algorithms and Applications*, 1st ed., Springer Nature, 2010.

[14]   N. Otsu, "Threshold Selection Method from Gray-Level Histograms," *IEEE Trans Syst Man Cybern,* vol. 9, no. 1, 1979, pp. 62-66.

[15]   G. W. Zack, W. E. Rogers, and S. A. Latt, "Automatic Measurement of Sister Chromatid Exchange Frequency," *J Histochem Cytochem,* vol. 25, no. 7, 1977, pp. 741-53.

[16]   I.-A. N. Costin-Anton Boiangiu, "Automatic Image Resampling Filter Generation"," *The Journal of Information Systems and Operations Management,* vol. 10, no. 2, 2016, pp. 487-502.

[17]   U. Erkan, L. Gökrem, and S. Enginoğlu, "Different Applied Median Filter in Salt and Pepper Noise," *Computers & Electrical Engineering,* vol. 70, 2018, pp. 789-798. https://doi.org/10.1016/j.compeleceng.2018.01.019

[18]   S. Paris, P. Kornprobst, and J. Tumblin, "A Gentle Introduction to Bilateral Filtering and Its Applications," ACM SIGGRAPH 2007 courses, 2007. https://doi.org/10.1145/1401132.1401134

[19]   P. Arbeláez, M. Maire, C. Fowlkes, and J. Malik, "Contour Detection and Hierarchical Image Segmentation," *IEEE Transactions on Pattern Analysis and Machine Intelligence,* vol. 33, no. 5, 2011, pp. 898-916. DOI: 10.1109/TPAMI.2010.161

[20]   G. Papari and N. Petkov, "Edge and Line Oriented Contour Detection: State of the Art," *Image and Vision Computing,* vol. 29, no. 2, 2011, pp. 79-103. https://doi.org/10.1016/j.imavis.2010.08.009

[21]   F. Akram, M. A. Garcia, and D. Puig, "Active Contours Driven by Local and Global Fitted Image Models for Image Segmentation Robust to Intensity Inhomogeneity," *PLOS ONE,* vol. 12, no. 4, 2017, p. e0174813. https://doi.org/10.1371/journal.pone.0174813

[22]   J. Norris, "Mach 8 High Reynolds Number Static Stability Capability Extension Using a Hypersonic Waverider at Aedc Tunnel 9," 25th AIAA Aerodynamic Measurement Technology and Ground Testing Conference, 2006.

https://doi.org/10.2514/6.2006-2815

[23]   G. Bradski, "The Opencv Library," *Dr. Dobb's Journal,* vol. 25, 2000, pp. 120-126.

[24]   L. Qin, Y. Xiang, S. Qin, and H. Liu, "On the Structures of Compressible Vortex Rings Generated by the Compressible

Starting Jet from Converging and Diverging Nozzles," *Aerospace Science and Technology,* vol. 106, 2020, pp. 106188.

https://doi.org/10.1016/j.ast.2020.106188